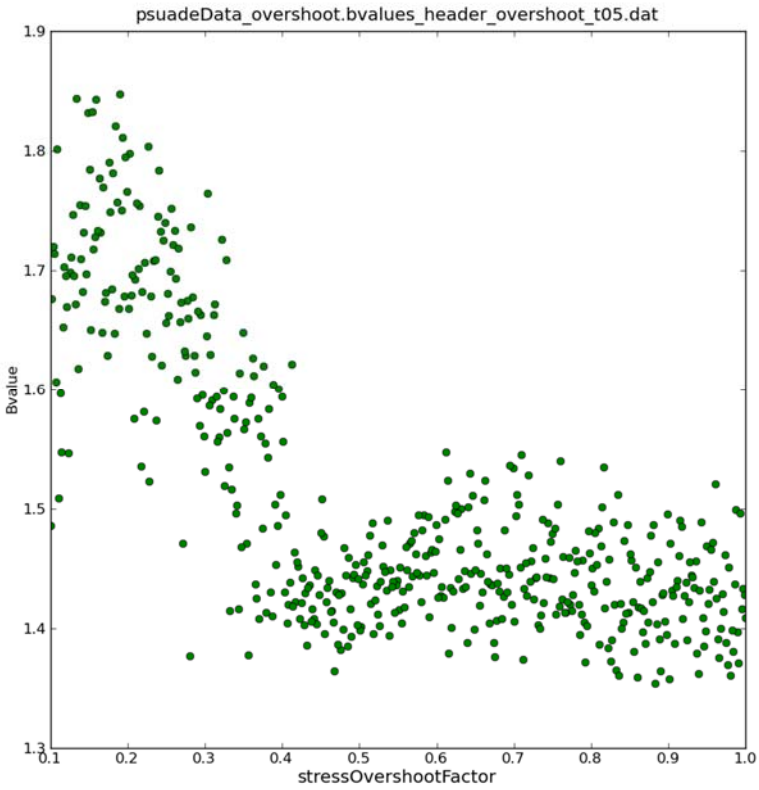

Parameter Sensitivity Analysis with the Seismicity Simulation Program RSQSim

28 January 2016

Office of Fossil Energy

NRAP-TRS-III-006-2016

Disclaimer

This report (LLNL-TR-615732) has been reviewed by Lawrence Livermore National Laboratory and approved for public release.

Cover Illustration: The cover shows the *b*-value as a function of the stress overshoot factor.

Suggested Citation: Trainor-Guitton, W.; Foxall, W.; Johnson, S. *Parameter Sensitivity Analysis with the Seismicity Simulation Program RSQSim*; NRAP-TRS-III-006-2016; NRAP Technical Report Series; U.S. Department of Energy, National Energy Technology Laboratory: Morgantown, WV, 2016; p 24.

An electronic version of this report can be found at:

http://www.netl.doe.gov/research/on-site-research/publications/featured-technical-reports

https://edx.netl.doe.gov/nrap

Parameter Sensitivity Analysis with the Seismicity Simulation Program RSQSim

Whitney Trainor-Guitton, William Foxall, Scott Johnson

Atmospheric, Earth and Energy Division, Lawrence Livermore National Laboratory, 7000 East Avenue, Livermore, CA 94551

NRAP-TRS-III-006-2016

Level III Technical Report Series

28 January 2016

This page intentionally left blank.

Table of Contents

This page intentionally left blank.

List of Figures

List of Tables

This page intentionally left blank.

Acronyms, Abbreviations, and Symbols

Term	Description
~	Approximately
μ_0	Base coefficient of friction
$\mu(V,\theta)$	Rate- and state-dependent coefficient of friction
σ	Fault normal stress
τ	Fault shear stress
A	Rate-and-state friction direct effect parameter (e.g. Marone, 1998)
a	Intercept parameter in relation $\log(N) = a - bM$ from Gutenberg and Richter (1954)
B	Rate-and-state evolution parameter
b (*b*-value)	Slope of the relation $\log(N) = a - bM$ from Gutenberg and Richter (1954)
dσ/dz	Normal stress gradient
D_c	Rate-and-state slip-weakening distance
θ	State variable (typical asperity lifetime)
θ_0	Reference state variable
g	Standard gravitational acceleration = 9.81 m s^{-2}
μ	Shear modulus
λ	Lamé's first parameter
M	Earthquake magnitude
N	Cumulative number of earthquakes
P	Pore pressure
V	Long-term fault slip rate
V_{eq}	Coseismic fault slip rate
3-D	Three-dimensional
DOE	U.S. Department of Energy
LBNL	Lawrence Berkeley National Laboratory
LLNL	Lawrence Livermore National Laboratory
m	Meter
CCS	Carbon capture and storage
NRAP	National Risk Assessment Partnership
PSHA	Probabilistic seismic hazard analysis
PSUADE	Computer code of Problem Solving Environment for Uncertainty Analysis and Design Exploration
RSQSim	**R**ate and **S**tate Earth**q**uake **Sim**ulator
TSI	Total Sensitivity Index

Acknowledgments

This work was completed as part of the National Risk Assessment Partnership (NRAP) project. Support for this project came from the U.S. Department of Energy's (DOE) Office of Fossil Energy's Crosscutting Research program. Support for this project came from the Department of Energy's (DOE) Office of Fossil Energy's Crosscutting Research program. The authors wish to acknowledge Traci Rodosta (Carbon Storage Technology Manager), Kanwal Majajan (Carbon Storage Division Director), M. Kylee Rice (Project Manager), Mark Ackiewicz (Division of CCS Research - Program Manager), Susan Maley and Steve Seachman (NETL Strategic Center for Coal), and Regis Conrad (DOE Office of Fossil Energy) for programmatic guidance, direction, and support.

The authors also wish to acknowledge Prof. Jim Dieterich and Dr. Keith Richards-Dinger at the University of California, Riverside for making the RSQSim earthquake simulation program available and for their continued interest and support.

ABSTRACT

Earthquake simulations performed using the program RSQSim as part of the National Risk Assessment Partnership's (NRAP) probabilistic seismic risk analyses depend on several parameters that are subject to degrees of uncertainty. In the current study, the sensitivity of simulation outputs to uncertainty in key RSQSim input parameters was analyzed using the Lawrence Livermore National Laboratory (LLNL) code PSUADE (Computer Code of Problem Solving Environment for Uncertainty Analysis and Design Exploration). A total sensitivity analysis was first performed to rank the parameters in terms of sensitivity, and then a detailed individual sensitivity analyses of the top-ranked parameters was conducted. The metric used to assess sensitivity is the Gutenberg-Richter *b*-value.

1. INTRODUCTION

A toolset for the analysis of the potential risks associated with induced seismicity resulting from carbon dioxide (CO_2) injection is being developed in support of the National Risk Assessment Partnership (NRAP). As described in the NRAP report, *First Generation Toolset for Calculation of Induced Seismicity Hazard Profiles* (Foxall et al., 2013), the toolset employs physics-based modeling using the code RSQSim developed by Jim Dieterich and Keith Richards-Dinger (Dieterich, 1995; Dieterich and Richards-Dinger, 2010; Richards-Dinger and Dieterich, 2012) to simulate earthquake sequences induced by elevated pore pressures as input to probabilistic seismic hazard assessment (PSHA) for induced seismicity.

RSQSim simulates earthquakes using a rate-and-state law that describes the evolution of the frictional shear strength of a fault, under constant-rate tectonic shear loading. The frictional strength, τ_s, is given by the Mohr-Coulomb relation:

$$\tau_s = \mu(\sigma - P) \tag{1}$$

where μ is the coefficient of friction, σ the normal stress on the fault, and *P* the pore pressure. Rate-and-state frictional laws have been empirically derived from laboratory experimental data, and provide the most complete description of earthquake nucleation and propagation currently available (e.g., Ben-Zion, 2008). According to these laws the frictional shear strength of a fault at a given time depends on the current slip rate, V, and variables that describe the "state" of the fault. The particular rate-and-state law employed in RSQSim contains a single state variable, θ, that has the dimensions of time and which is interpreted as the typical lifetime of the asperities at which the two sides of the fault are in contact. The law can be written as:

$$\mu(V,\theta) = \mu_0 + A\ln\left(\frac{V}{V_0}\right) + B\ln\left(\frac{\theta}{\theta_0}\right), \tag{2}$$

where μ is the current coefficient of friction, μ_0, V_0 and θ_0 are reference (base) values of the coefficient of friction, slip rate, and state variable, respectively, and *A* and *B* are material constants. At constant fault normal stress, the state variable evolves with time and slip according to:

$$\frac{\partial\theta}{\partial t} = 1 - \frac{\theta V}{D_c}, \tag{3}$$

where D_c is the characteristic slip distance (a material property) over which θ evolves at the new slip rate. From Equation 2, the response to a step change in slip rate is an initial, instantaneous increase in fault strength governed by the constant *A* (the *rate* effect) followed by a drop in strength to a final value μ over slip distance D_c (the *state* effect). The net effect depends on the relative values of *A* and *B*. If *B*>*A* (*B*-*A* positive) then slip-weakening and slip acceleration occurs that can lead to the nucleation of unstable slip in an earthquake. Conversely, if *B*<*A* (*B*-*A* negative) then the fault is slip-strengthening and only stable, aseismic sliding can occur.

RSQSim simulations are carried out on faults divided into elements and under specified initial shear and normal stress conditions. Long-term tectonic shear stress loading is applied at a constant rate. At each time step through the simulation the rate-and-state law is applied to each

element to determine its slip status. When coseismic slip nucleates on an element, the resulting normal and shear stress changes are transmitted to all of the other elements using a boundary-element method. These coseismic stress changes can cause seismic slip to nucleate on neighboring elements, thus producing a cascade of failures in a propagating, multi-element rupture. Therefore, the simulation produces the full range of earthquake magnitudes between the lower and upper bounds set by the size of the elements and the overall dimensions of the fault, respectively.

The objective of the present study was to examine the sensitivity of earthquake simulations to the rate-and-state parameter values that are input to RSQSim. Overall initial bounds on the parameters are adopted from the literature. However, application of the rate-and-state laws produces a rich and complex variety of earthquake frequency-size behaviors, and determining appropriate bounds on most of the parameters remains the subject of vigorous ongoing research (e.g. Marone, 1998; Ampuero and Rubin, 2008; Fang et al., 2011). In particular, significant questions remain regarding the scaling of the laboratory-derived parameters A, B, and D_c to earthquake dimensions and crustal conditions. Furthermore, RSQSim uses two methods (outlined below) to approximate elastodynamic effects during earthquake rupture that are not captured by the rate-and-state law, and it is especially important to assess the influence of these approximations on the simulation results.

While the rate-and-state law provides an adequate description of the quasi-static process by which earthquakes nucleate and are arrested—and hence the seismic cycle that produces earthquake sequences—it does not represent the full elastodynamics of coseismic fault rupture over the order of seconds duration of the actual earthquake; i.e. the law does not give a description of dynamic earthquake slip and the generation of seismic waves. RSQSim provides a first order approximation of the elastodynamic effects using two correction parameters (Richards-Dinger and Dieterich, 2012). The first parameter addresses the observation in fully dynamic simulations of earthquake rupture (e.g. Madariaga, 1976) that the stress drop during an earthquake overshoots the sliding frictional level predicted by quasi-static calculations. Therefore, the stress on a fault element during dynamic coseismic slip is generally lower than predicted by the rate-and-state law. RSQSim mimics this by applying a stress overshoot factor, s, specified as an input parameter, that governs the stress level at which coseismic slip ceases and the element heals.

The second parameter corrects for the tendency of RSQSim simulations to underestimate the dynamic stress concentration at the edge of an element induced by the rupture of the element (which nucleates at the center). This makes it unrealistically difficult to overcome the resistance to rupture of adjoining elements posed by the A (strengthening) term in the first equation above, hence inhibiting multi-segment ruptures and larger earthquakes. This problem is particularly acute when large elements (~km) are used to simulate large tectonic earthquakes (Richards-Dinger and Dieterich, 2012), but should be less so for the smaller elements (~10–100 m) used in our simulations of typically smaller induced earthquakes. To address this problem, RSQSim temporarily reduces the A values in elements adjacent to elements undergoing seismic slip by a factor $fA < 1$, specified as an input parameter.

Although these two corrections, and particularly the latter, are somewhat *ad hoc*, appropriate ranges of both the stress overshoot and fA parameters have been calibrated to some extent by comparison of RSQSim results with fully dynamic simulations (Dieterich and Richards-Dinger, 2010; Richards-Dinger and Dieterich, 2012).

Table 1: Initial parameter ranges used for the Latin hypercube sampling

Parameter/Symbol	Central Value	Range	Data source
Base coefficient of friction, μ_0	---	0.6 to 0.9	Assumed
Lamé's first parameter, λ	18034 MPa	Constant	Derived from KB-502 well logs
Shear modulus, μ	9290 MPa	Constant	Derived from KB-502 well logs
Reference state variable, θ_0	---	10^8 to 10^9 s	Assumed
Fault normal stress, σ	17 MPa	Constant	Derived from KB-502 well data
Normal stress gradient with Depth, $d\sigma/dz$	0.02 MPa m^{-1}	Constant	Derived from KB-502 well data
Fault shear stress, τ	4.0 MPa	Constant	Derived from KB-502 well data
Long-term fault slip rate, V	1 mm y^{-1}	Constant	Assumed
Fault length	1.6 km	Constant	In Salah 3-D seismic data
Fault width	1.5 km	Constant	Assumed
Rate-and-state friction direct effect parameter, A	0.005	0.001 to 0.01	Generic values (e.g. Marone, 1998)
Rate-and-state evolution parameter, B	0.015	Constant (i.e., varying A/B)	Assumed
Rate-and-state slip-weakening distance, D_c	25 x 10^{-6}m	Constant	Assumed
Reduction factor for A, fA,	0.2	0.1 to 0.5	Calibrated with fully dynamic simulations (Richards-Dinger and Dieterich, 2012)
Stress overshoot factor, s	0.5	0.1 to 1.0	Madariaga (1976); Calibrated with fully dynamic simulations (Richards-Dinger and Dieterich, 2012)
Coseismic fault slip velocity, V_{eq}	1 m s^{-1}	Constant	Representative generic value

2. METHOD

2.1 SAMPLING WITH PSUADE

Lawrence Livermore National Laboratory's (LLNL) PSUADE (Problem Solving Environment for Uncertainty Analysis and Design Exploration) code has been developed to assist with validating simulation models (Tong, 2009). Specifically, PSUADE was used to: 1) sample the ranges of possible values (uncertainty distributions) for the most uncertain parameters; 2) assess which variables have the most influence on the output of the simulations; and 3) assess the sensitivity of the simulations to uncertainties in individual parameters. PSUADE allows for "non-intrusive" (i.e. the simulation codes do not need to be modified) uncertainty quantification by introducing possible probability distributions of input parameters to a selected simulation model, in this case RSQSim. PSUADE's Latin hypercube sampling capability (see McKay et al., 1979 for full description) was utilized to represent discretely the distributions of the input parameters. The Latin hypercube sampling divides the distribution of each input variable into equally spaced bins, such that the same number of data points populates each bin.

2.2 DEPENDENT VARIABLE METRIC

The frequency-magnitude statistics of earthquake occurrence in a region is generally observed to follow the Gutenberg-Richter relation (Gutenberg and Richter, 1954) over at least some substantial portion of the magnitude range. The relationship is:

$$\log(N) = a - bM \tag{4}$$

where N is the cumulative number of earthquakes per year having magnitudes greater than or equal to M, and the parameters a and b are constants. Therefore, a plot of log(N) versus M is linear with (negative) slope b. The constant a (the intercept on the log(N) axis at M=0) expresses the overall level of earthquake occurrence. Note that the plot will be linear above some lower magnitude threshold, below which the apparent occurrence frequencies fall off because of incomplete detection by the seismic monitoring network. A high value of b (or b-value) indicates a high frequency of small events relative to large events and vice versa. Regional b-values for tectonic earthquakes are almost always close to 1. Under certain conditions, such as in volcanic areas or under the influence of fluid pore pressure changes, b-values can be significantly higher, but they are rarely observed to be much above 2. In certain regions, earthquakes towards the upper end of the magnitude range appear to occur more frequently than predicted by extrapolating the linear Gutenberg-Richter plot from lower magnitudes.

Earthquake occurrence on individual fault segments often follow the Gutenberg-Richter law at lower magnitudes but show distinctly enhanced frequencies around larger "characteristic" earthquakes (Schwartz and Coppersmith, 1984; Ben-Zion, 2008) that rupture essentially across the entire segment. The frequency-magnitude plot for this characteristic earthquake model (Youngs and Coppersmith, 1985) can be approximated by three segments: 1) a relatively steep linear segment corresponding to a truncated Gutenberg-Richter distribution at lower magnitudes above the detection threshold; 2) a flatter linear segment over some intermediate magnitude range; and 3) a steep roll-off within the magnitude range of the characteristic earthquakes.

RSQSim simulations exhibit the full range of frequency-magnitude behavior described above, depending on the input parameters (the magnitude detection threshold corresponds in this case to the smallest event simulated by the rupture of a single element). The b-slopes and the magnitude

at the intersection of Segments 1 and 2 on Gutenberg-Richter plots are generally used to characterize the seismicity within a region or on an individual fault. The present study used the linear *b*-slope fit over the lower magnitude range, which is unaffected by boundary or truncation effects, as the metric (i.e., dependent variable) in comparing simulation outputs and assessing parameter sensitivity. Future work will include the complete frequency magnitude characterization in the sensitivity analyses by using the *b*-slope of the intermediate magnitude range when bi-linear behavior is simulated, the magnitude at which the change in *b*-slope occurs and the upper bound magnitude as additional metrics.

2.3 TOTAL AND INDIVIDUAL SENSITIVITY ANALYSES

As discussed in the Introduction and summarized in Table 1, RSQSim requires several input parameters. Some of these are relatively well constrained, but others are less so. The first goal of the sensitivity study is to determine which parameters have greater influence on the output of the simulation model. This was accomplished through the use of the PSUADE's Total Sensitivity Analysis functionality to rate the influence of different parameters on the metric, the *b*-value. By concurrently varying multiple input parameters, the relative or total sensitivity of the resulting *b*-values can be evaluated. PSUADE makes use of Sobol's sensitivity analysis, which is a variance-based method that compares the correlation between outputs of pairs of sample points that differ by a single dimension of the input. A large correlation between these two sets of outputs (due to variations in the single dimension of input) indicates that that particular input does little to alter the output and thus it is less significant (Saltelli et al., 2004). The output from the Sobol analysis is in the form of a Total Sensitivity Index (TSI) for each input parameter. The TSIs are used to rank the parameter sensitivities relative to each other (Tong, 2010).

Individual sensitivity analyses for the four parameters having the highest TSIs were performed using PSUADE to sample the uncertainty distribution of each input parameter and produce plots of the resulting *b*-values across the parameter range. These plots were used to assess the systematic variation in *b* with respect to variations in the parameters. Parameter ranges that yield unrealistic *b*-values can then be removed from the input distributions, thus narrowing the uncertainty in simulation outputs.

2.4 FAULT GEOMETRY

A planar fault with a length of 2,000 m and height of 1,560 m, was used for these simulations. The top of the fault was modeled at a depth of 850 m. The element size was set at 40 m. The strike, dip, and rake of the vertical, left-lateral strike-slip fault were set at 0, 90, and 0-degrees respectively. The fault was given a slip rate of 3.1e-11 m/s.

3. RESULTS AND DISCUSSION

Initial ranges were established for the model input parameters listed in Table 1 based on field data and available published information. The hypothetical fault model and associated material properties are described in Foxall et al. (2012). Representative values for elastic moduli are derived from P- and S-wave velocity logs measured in well KB-502 at the In Salah CCS site in Algeria (e.g. Vasco et al., 2010). Stress data are taken from an unpublished stress analysis for KB-502 performed by the In Salah Joint Industrial Partnership. The parameters having the highest uncertainty were selected for sensitivity analysis. All of the selected parameters are discussed in the Introduction.

3.1 TOTAL SENSITIVITY INDEX

All parameters are sampled from uniform distributions over the ranges given in Table 2. To calculate TSI, all parameters were varied simultaneously, yielding a full description of the metric variance as a function of the total parameter space. The resulting TSI and overall relative ranking for each input parameter is shown in the last two columns of the table.

Table 2: Parameter ranges used for TSI and sensitivity ranking

Parameter	Value	Total Sensitivity (Correlation Coefficient)	Rank
Stress overshoot factor, s	0.1–1.0	0.82	1
Rate-and-state friction direct effect parameter, A	0.001–0.01	0.23	2
Reduction factor for A, fA	0.1–0.5	0.17	3
Base coefficient of friction, μ_0	0.6–0.9	0.12	4
Reference state variable, θ_0	10^8–10^9 s	0.027	5

The total sensitivity analysis shows that the *b*-value varies almost independently of θ_0, while it varies strongly with the stress overshoot factor, *s*.

3.2 INDIVIDUAL SENSITIVITY ANALYSES

For all of the individual sensitivity analyses described below, except the last (see section 3.2.4), the base coefficient of friction, μ_0, assigned to each fault element was randomly sampled from a uniform distribution over the commonly accepted range 0.6–0.9 (Byerlee, 1978). This provided the stochastic background distribution (roughness) of shear strength across the fault plane required to obtain physically realistic earthquake frequency-magnitude distributions (e.g. Ben-Zion, 2008).

3.2.1 Stress Overshoot Factor

The parameter with highest TSI is the Stress Overshoot Factor, *s*. Figure 1 shows that although *b* for all values of *s* is within a range consistent with values generally derived from observations of regional and induced seismicity, there is a very pronounced sensitivity to *s* values between 0.1 and 0.45 that is higher than the average TSI indicates. Richards-Dinger and Dieterich (2012) suggest that small values of *s* allow an element that has just slipped to be re-triggered under

stressing from continuing rupture on adjacent patches. The re-stressing can outpace fault healing so that the element quickly fails again, which can lead to the continuous slip at slower slip speeds over broad regions that is characteristic of crack-like ruptures. Conversely, large *s* values favor healing outpacing re-stressing, leading to a single episode of slip on an element so that the ruptures are more pulse-like.

The break in the sensitivity curve at an *s* value of 0.4–0.45 is consistent with the theoretical 0.35–0.4 upper bound of *s* for an expanding circular shear crack (e.g. Madariaga, 1976). This and the break in sensitivity were tentatively interpreted as evidence that the lower the value of *s* the higher the stress level remaining on an element at the end of slip, and therefore the closer the element remains to incipient failure. This not only leads to more frequent events, since little loading is required from slip on nearby patches to recommence failure, but these events also remain small, as the released energy is not large enough to lead to progressive failure (i.e., an expanding rupture front) past the local area of the initiating rupture. This results in relatively large *b*-values. This interpretation is supported by Figure 2. This figure shows the magnitude at the intersection of *b*-slope segments 1 and 2 (Section 2.2) plotted against *s*, and illustrates that the change in slope takes place at a higher magnitude for larger values of *s*. (The horizontal banding seen in Figure 2 is likely related to the discretization of the mesh.)

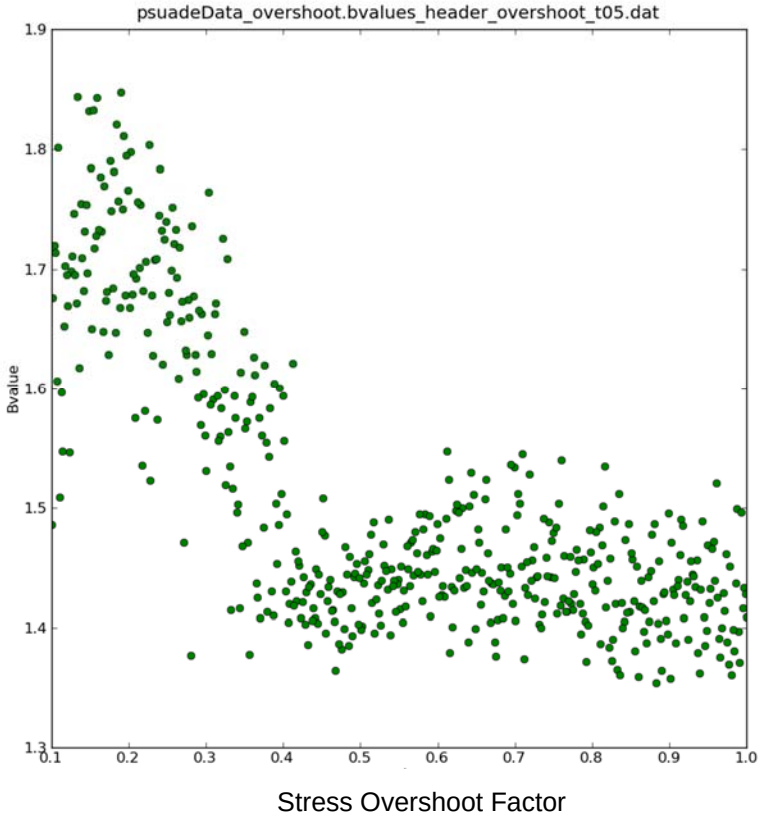

Note: Scatter due to stochastic distribution of base friction coefficient.

Figure 1: b-value as a function of stress-overshoot factor.

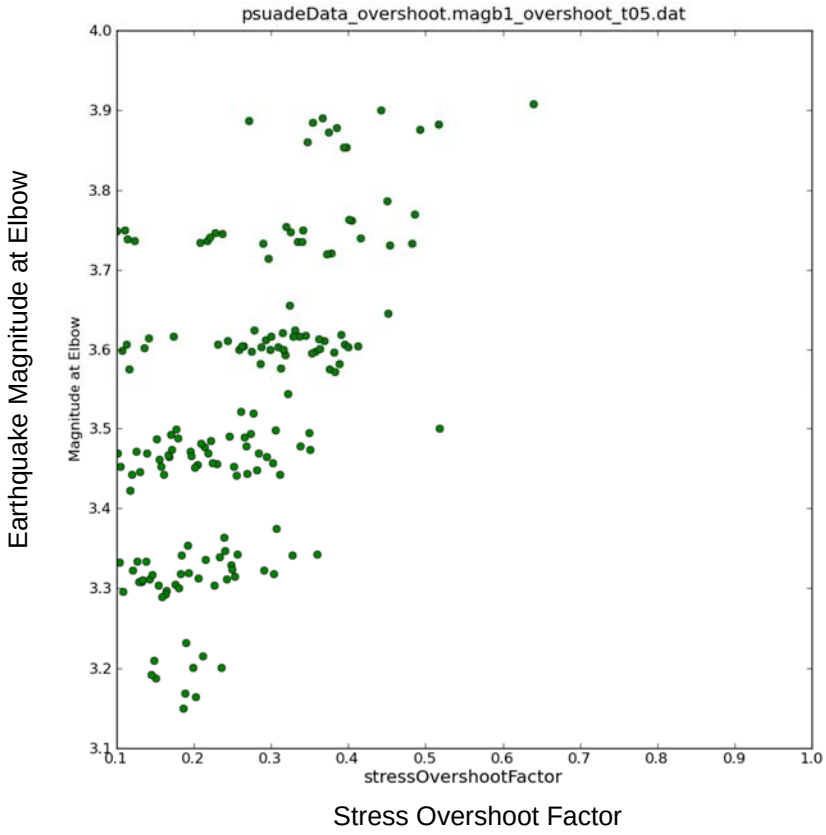

Note: Scatter due to stochastic distribution of base friction coefficient.

Figure 2: Earthquake magnitude at elbow as a function of stress-overshoot factor.

3.2.2 *A/B* Ratio

The parameter with the second highest TSI is the *A* parameter in the rate-and-state friction model (Section 1). It is found that simulation results are not very sensitive to variations in the *B* parameter alone, so in the present analysis the *B* parameter is held constant. Therefore, varying *A* is equivalent to varying the ratio *A/B*. This parameterization was selected because discussions in the literature (e.g. Fang et al., 2011; Ampuero and Rubin, 2008) generally revolve around the effects of variations in *A/B* and (*B*-*A*).

As the value of *A* approaches *B* the stress drop in a seismic slip event approaches zero, and the failure profile approaches that of a simple Coulomb frictional surface. As such, one would expect that all failures would be relatively localized, resulting in a high *b*-value, consistent with what is seen in Figure 3.

A/B ratios discussed in the literature range from 1/15 (e.g. Dieterich, 1995; Marone, 1998) to as high as 8/9 (Dieterich and Richards-Dinger, 2010). However, Figure 3 shows that ratios higher than about 0.6 result in unrealistically high *b*-values and appear to approach infinity asymptotically. At these high values the fault contact becomes akin to a simple sliding surface with no events larger than the minimum magnitude dictated by the element size.

Laboratory measurements reported by Dieterich (1995) restrict the *A/B* to be less than about 2/3, consistent with the behavior shown in Figure 3. Between ~0.1 and 0.55 *b* is almost insensitive to the value of *A/B*, showing only a small monotonic increase over this range.

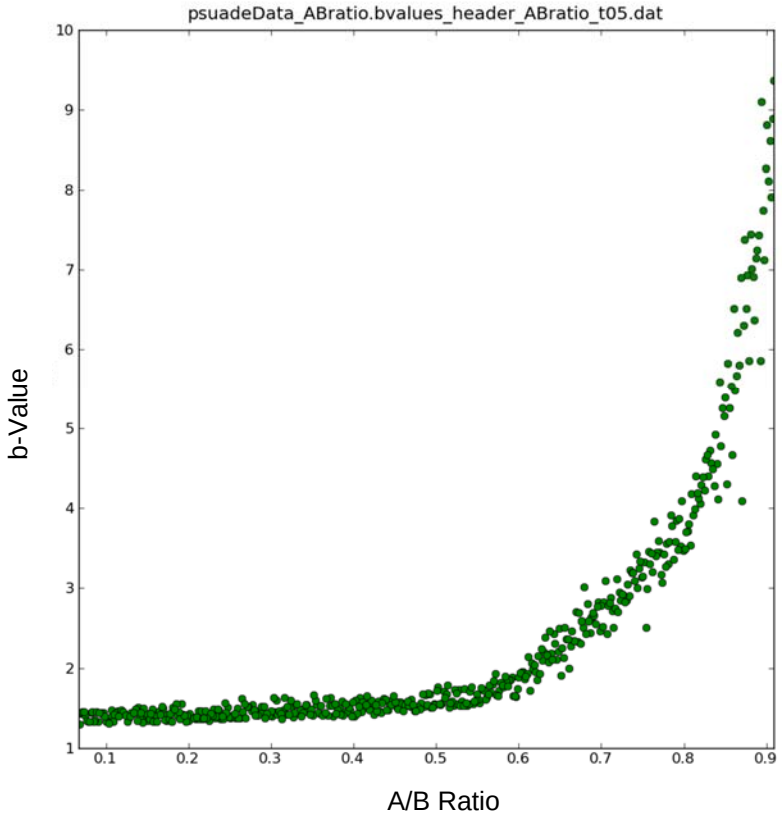

Note: Scatter due to stochastic distribution of base friction coefficient.

Figure 3: b-value as a function of A/B ratio.

3.2.3 fA

The parameter with the third highest TSI is *fA*, the A reduction parameter. A more physically appropriate formulation for this parameter would be akin to a stress intensity factor in fracture mechanics, in which case it would depend both on element size and nucleation length; the nucleation length is a function of D_c, (*B*-*A*), normal stress, and shear modulus (Dieterich, 1995). In general, for a discrete problem of the type dealt with here, the mesh size must be significantly greater than the nucleation length, so that any event nucleates within a single element. In the present sensitivity studies, the nucleation length is approximately 10 m, while the element size is 50 m.

The effective rate coefficient *A* becomes larger with increasing *fA*. Therefore, it is not surprising that a similar trend is seen for *fA* (Figure 4) as for *A/B* (Figure 3), although not as extreme. This reflects the fact that larger effective values of *A* (relative to *B*) result in more numerous, smaller events and thus higher *b*-values. That is, as rate-effects overwhelm state effects, the rupture distribution skews towards smaller magnitude, more frequent seismicity.

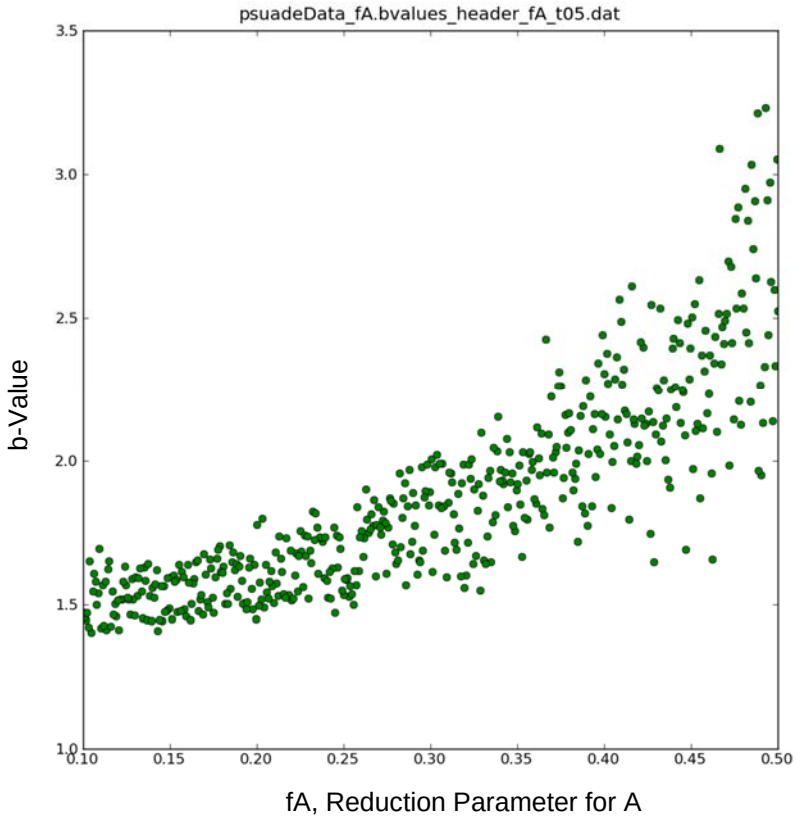

Figure 4: *b*-value as a function of the A-parameter reduction factor.

3.2.4 Base Coefficient of Friction

Sensitivity to the value of the base coefficient of friction μ_0 was also investigated. The initiation of this study assumed the distribution of this parameter could be used as a surrogate for the geometry of the fault (relative to the in situ stress field), as both have dominant impact on the shear strength as a function of position on the fault plane. However, the sensitivity result shown in Figure 5 provides a striking illustration of how this assumption may be flawed. Although the case of a flat fault having constant coefficient of friction simulated with the RSQSim methodology is pathological, it may be capturing the combined effects of geometry and friction. That the *b*-values seem to be independent of the base coefficient of friction (as calculated at late time, after the so-called "burn-in" period, after which the statistics become stationary) also indicates a Lyanpunov instability resultant in accumulated chaotic changes. This is instructive in terms of understanding the effects and points to the need to perform an analogous study that focuses on the effect of geometric heterogeneity on the fault.

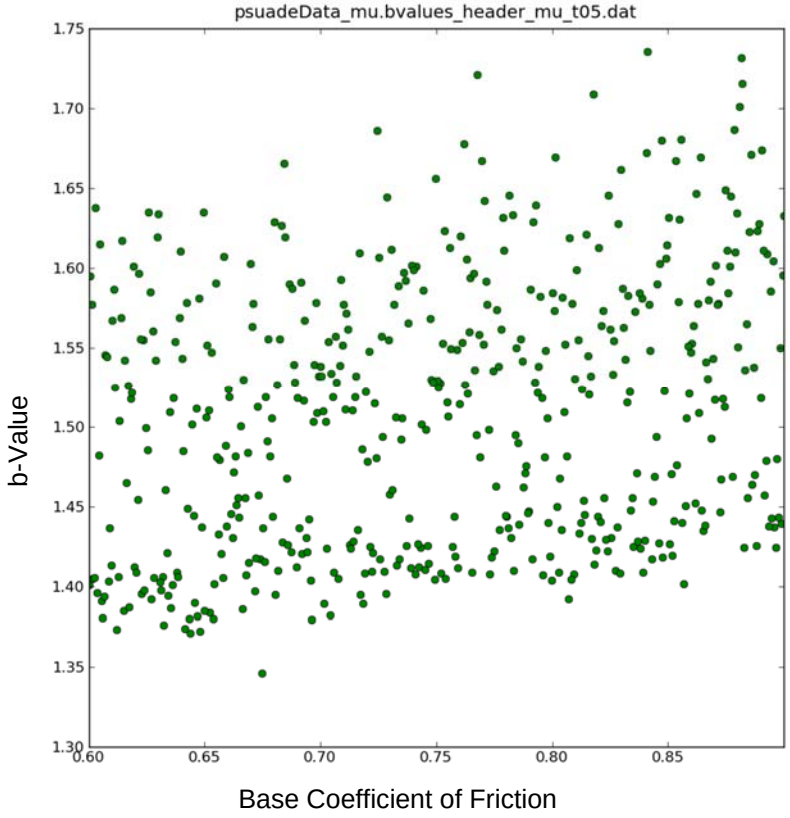

Figure 5: *b*-value as a function of the constant value of the base coefficient of friction.

4. CONCLUSIONS

In this study, both a total sensitivity analysis as well as individual sensitivity analyses was completed on parameters identified by high Total Sensitivity Index (TSI). In aggregate, the results show that both *A* and *B* (rate versus state) effects and sensitivity to elastodynamic approximations are dominant. These can be broken down into individual effects related to stress overshoot factor, *A/B* ratio, and the *A* reduction factor, *fA*, as detailed in the preceding results and discussion.

Future efforts will now be focused on obtaining better constraints on the three parameters of the rate-and-state law. Although *A* and *B* are uniquely associated with the fault material properties, *fA* is purely a numerical factor. In order to constrain this parameter, more work must be done on determining the dependence of the stressing of element boundaries on mesh size and nucleation length. Finally, possible correlations among the parameters were not yet considered. Assessment of sensitivity that considers such correlations can be approached through principle component analysis (Scheidt and Caers, 2009).

This page intentionally left blank.

5. REFERENCES

Ampuero, J-P.; Rubin, A. Earthquake Nucleation on Rate and State Faults – Aging and slip laws. *J. Geophys. Res*. **2008,** *113*.

Ben-Zion, Y. Collective Behavior of Earthquakes and Faults: Continuum-discrete Transitions, Progressive Evolutionary Changes, and Different Dynamic Regimes. *Rev. Geophys.* **2008,** *46*, 70.

Byerlee, J. Friction of Rocks. *Pure Appl. Geophys.* **1978,** *116*, 615–626.

Dieterich, J. Earthquake Simulations with Time-dependent Nucleation and Long-range Interactions. *Nonlinear Processes in Geophysics* **1995,** *2*, 109–120.

Dieterich, J.; Richards-Dinger, K. Earthquake Recurrence in Simulated Fault Systems. *Pure Appl. Geophys.* **2010,** *167*, 1087–1104.

Fang, Z.; Dieterich, J.; Richards-Dinger, K. Earthquake Nucleation on Faults with Nonconstant Normal Stress, *J. Geophys. Res*. **2011,** *116*.

Foxall, W.; Hutchings, L.; Johnson, S.; Savy, J. *First-Generation Toolset for Calculation of Induced Seismicity Hazard Profiles*; NRAP-TRS-III-002-2013; NRAP Technical Report Series; U.S. Department of Energy, National Energy Technology Laboratory: Morgantown, WV, 2012; p 16. http://netl.doe.gov/nrap/NRAP-TRS-III-002-2013_Induced%20Seismicity.20130117.pdf

Gutenberg, B.; Richter, C. F. *Seismicity of the Earth and Associated Phenomena*, 2nd ed.; Princeton Univ. Press: Princeton, NJ, 1954.

Madariaga, R. Dynamics of an Expanding Circular Fault. *Bull. Seismol. Soc. Am*. **1976**, *66*, 639–666.

Marone, C. Laboratory-derived Friction Laws and their Application to Seismic Faulting. *Annu. Rev. Earth. Planet. Sci.* **1998,** *26*, 643–696.

McKay, M.; Beckman, R.; Conover, W. A Comparison of Three Methods for Selecting Values of Input Variables in the Analysis of Output from a Computer Code. *Technometrics* **1979,** *21*, 239–245.

Richards-Dinger, K.; Dieterich, J. RSQSim Earthquake Simulator. *Seismol. Res. Lett*. **2012,** *83*, 983–990.

Saltelli, A.; Tarantola, S.; Campolongo, F.; Ratto M. *Sensitivity Analysis in Practice: A Guide to Assessing Scientific Models*; John Wiley and Sons, Ltd., 2004.

Schwartz, D. P.; Coppersmith, K. J. Fault Behavior and Characteristic Earthquakes: Examples from the Wasatch and San Andreas Fault Zones. *J. Geophys. Res.* **1984,** *89*, 5681–5698.

Scheidt, C.; Caers, J. Representing Spatial Uncertainty Using Distances and Kernels. *Mathematical Geosciences* **2009,** *41*, 397–419.

Tong, C. *PSUADE User's Manual* (Version 1.2.0); LLNL-SM-407882; Lawrence Livermore National Laboratory: Livermore, CA, 2009. http://computation.llnl.gov/casc/uncertainty_quantification/

Tong, C. Self–validated Variance–based Methods for Sensitivity Analysis of Model Outputs. *Reliab. Eng. Syst. Safe.* **2010,** *95*, 301–309.

Vasco, D. W.; Rucci, A.; Ferretti, A.; Novali, F.; Bissel, R. C.; Ringrose, P. S.; Mathieson, A. S.; Wright, I. W. Satellite-based Measurements of Surface Deformation Reveal Fluid Flow

Associated with the Geological Storage of Carbon Dioxide. *Geophys. Res. Let*. **2010**, *37*. DOI:10.1029/2009GL041544.

Youngs, R.; Coppersmith, K. Implications of fault Slip Rates and Earthquake Recurrence Models to Probabilistic Seismic Hazard Estimates. *Bull. Seismol. Soc. Am*. **1985,** *76*, 939–964.

NRAP is an initiative within DOE's Office of Fossil Energy and is led by the National Energy Technology Laboratory (NETL). It is a multi-national-lab effort that leverages broad technical capabilities across the DOE complex to develop an integrated science base that can be applied to risk assessment for long-term storage of carbon dioxide (CO_2). NRAP involves five DOE national laboratories: NETL, Lawrence Berkeley National Laboratory (LBNL), Lawrence Livermore National Laboratory (LLNL), Los Alamos National Laboratory (LANL), and Pacific Northwest National Laboratory (PNNL).

Technical Leadership Team

Diana Bacon
Lead, Groundwater Protection Working Group
Pacific Northwest National Laboratory
Richmond, WA

Jens Birkholzer
LBNL Lab Lead
Lawrence Berkeley National Laboratory
Berkeley, CA

Grant Bromhal
Technical Director, NRAP
Research and Innovation Center
National Energy Technology Laboratory
Morgantown, WV

Chris Brown
PNNL Lab Lead
Pacific Northwest National Laboratory
Richmond, WA

Susan Carroll
LLNL Lab Lead
Lawrence Livermore National Laboratory
Livermore, CA

Abdullah Cihan
Lead, Reservoir Performance Working Group
Lawrence Berkeley National Laboratory
Berkeley, CA

Tom Daley
Lead, Strategic Monitoring Working Group
Lawrence Berkeley National Laboratory
Berkeley, CA

Robert Dilmore
NETL Lab Lead
Research and Innovation Center
National Energy Technology Laboratory
Pittsburgh, PA

Nik Huerta
Lead, Migration Pathways Working Group
Research and Innovation Center
National Energy Technology Laboratory
Albany, OR

Rajesh Pawar
LANL Lab Lead
Lead, Systems/Risk Modeling Working Group
Los Alamos National Laboratory
Los Alamos, NM

Tom Richard
Deputy Technical Director, NRAP
The Pennsylvania State University
State College, PA

Josh White
Lead, Induced Seismicity Working Group
Lawrence Livermore National Laboratory
Livermore, CA

Sean Plasynski
Executive Director
Technology Development and
Integration Center
National Energy Technology Laboratory
U.S. Department of Energy

Heather Quedenfeld
Associate Director
Coal Development and Integration
National Energy Technology Laboratory
U.S. Department of Energy

Traci Rodosta
Technology Manager
Strategic Planning
Science and Technology Strategic Plans
and Programs
National Energy Technology Laboratory
U.S. Department of Energy

Mark Ackiewicz
Director
Division of Carbon Capture and Storage
Office of Fossil Energy
U.S. Department of Energy